Molecular Therapy
Nucleic Acids
Original Article

Alleviation of Toxicity Caused by Overactivation of P*parα* through P*parα*-Inducible miR-181a2

Yanjie Cheng,[1,2] Zhuying Wei,[3] Shengsong Xie,[1] You Peng,[1] Yi Yan,[1,2] Dan Qin,[1,2] Shenghui Liu,[1,2] Yanling Xu,[1,2] Guangpeng Li,[3] and Lisheng Zhang[1,2]

[1]College of Veterinary Medicine, Huazhong Agricultural University, Wuhan 430070, China; [2]Bio-medical Center, Huazhong Agricultural University, Wuhan 430070, China; [3]The Key Laboratory of Mammalian, Reproductive Biology and Biotechnology of the Ministry of Education, College of Life Sciences, Inner Mongolia University, Hohhot, China

Widely varied compounds, including certain plasticizers, hypolipidemic drugs (e.g., ciprofibrate, fenofibrate, WY-14643, and clofibrate), agrochemicals, and environmental pollutants, are peroxisome proliferators (PPs). Appropriate dose of PPs causes a moderate increase in the number and size of peroxisomes and the expression of genes encoding peroxisomal lipid-metabolizing enzymes. However, high-dose PPs cause varied harmful effects. Chronic administration of PPs to mice and rats results in hepatomegaly and ultimately carcinogenesis. Nuclear receptor protein peroxisome proliferator-activated receptor-α (P*parα*) was shown to be required for this process. However, biological adaptations to minimize this risk are poorly understood. In this study, we found that miR-181a2 expression was induced by the P*parα* agonist WY-14643. Moreover, exogenous expression of miR-181a-5p dramatically alleviated the cell toxicity caused by overactivation of P*parα*. Further studies showed that miR-181a-5p directly targeted the P*parα* 3′ untranslated region and depressed the P*parα* protein level. This study identified a feedback loop between miR-181a-5p and P*parα*, which allows biological systems to approach a balance when P*parα* is overactivated.

INTRODUCTION

Certain plasticizers, hypolipidemic fibrate drugs, environmental pollutants, and natural products are peroxisome proliferators (PPs).[1–3] Known or unknown PPs are widely distributed in the environment, and it is inevitable for people to come into contact with them. Appropriate dose of PPs usually results in moderate increase in the number and size of peroxisomes and the expression of genes encoding peroxisomal lipid-metabolizing enzymes, and certain PPs (e.g., ciprofibrate and fenofibrate) are hypolipidemic drugs.[4,5] However, high-dose WY-14643 may cause varied harmful effects. It has been reported that long-term exposure of rodents to WY-14643 leads to increases in peroxisomes, cell proliferation, oxidative damage, and ultimately resulting in the development of hepatic adenomas and carcinomas. Proliferator-activated receptor-α (P*parα*) was shown to be required for these pleiotropic responses.[6]

P*parα* is a nuclear receptor (NR) protein encoded by the P*parα* gene.[7] NRs are ligand-inducible transcription factors that alter transcription rates, as well as the subsequent expression levels of their target genes by contacting their promoter or enhancer sequences at specific recognition sites.[8–10] P*parα* is activated by PPs, and in response to PPs activation, P*parα* heterodimerizes with retinoid X receptor α (R*xrα*).[11,12] Additionally, after the recruitment of co-activators, P*parα* binds to the peroxisome proliferator response element (PPRE) in the promoter or enhancer region of those downstream target genes.[12,13] In addition, P*parα* regulates the expression of non-coding RNAs, such as microRNAs (miRNAs).[14] Previous reports demonstrated that P*parα* is involved various cellular processes, including lipid metabolism, inflammatory responses, autophagy, and apoptosis.[15–18] P*parα* activators induce apoptosis of activated macrophages and then contribute to the treatment of atherosclerosis.[16] Cardiac-specific overexpression of P*parα* in mice contributes to the development of cardiac dysfunction. It is partially because of the generation of harmful reactive oxygen species (ROS) produced by increased mitochondrial flux.[19] This excess of ROS may further cause various cytotoxic effects. Then, what is the underlying mechanism of biological systems to balance the harmful effects caused by P*parα* overactivation?

miRNAs are genomically encoded small non-coding RNAs that regulate the flow of genetic information through base pairing between the miRNA seed sequence (5′ nucleotides 2–8) and 3′ untranslated regions (3′ UTRs) of mRNAs, causing mRNA degradation, translation inhibition, or both.[20–23] The human miR-181 family constitutes four members (miR-181a, miR-181b, miR-181c, and miR-181d).[24] They are encoded by three different transcripts located on three different chromosomes. MiR-181a and miR-181b are clustered together on two genomic locations: the human miR-181-a1 and miR-181-b1 cluster being located on chromosome 1, and the miR-181a2 and miR-181b2 cluster being located on chromosome 9. The miR-181c and

Received 18 December 2016; accepted 21 September 2017;
https://doi.org/10.1016/j.omtn.2017.09.008.

Correspondence: Lisheng Zhang, College of Veterinary Medicine, Huazhong Agricultural University, Wuhan 430070, China.
E-mail: lishengzhang@mail.hzau.edu.cn
Correspondence: Guangpeng Li, The Key Laboratory of Mammalian, Reproductive Biology and Biotechnology of the Ministry of Education, College of Life Sciences, Inner Mongolia University, Hohhot, China.
E-mail: guangpengli@imu.edu.cn

miR-181d cluster is located on chromosome 19.[24] Recently, the transcriptional level regulation of the miR-181 family has received extensive concerns. Chemotherapeutic drug doxorubicin treatment significantly increased the expression of miR-181a1 in breast cancer cells, which enhanced breast cancer cell survival by targeting pro-apoptosis gene B*ax*.[25] Induction of miR-181a upon cisplatin treatment was shown to enhance apoptosis in non-small-cell lung cancer A549 cells.[26] Our work revealed that miR-181a2 expression was induced by high-dose P*parα* agonist WY-14643.

In this study, we analyzed and evaluated the relationship among the overactivation P*parα*, miR-181a-5p expression, and cytotoxicity. Our data showed that P*parα* agonists induced miR-181a-5p transcription and that miR-181a-5p repressed P*parα* expression through partial base pairing with its 3′UTR, forming a feedback loop in the regulation of high-dose WY-14643-induced cytotoxicity, and miR-181a-5p reduced the occurrence of high-dose WY-14643-induced cytotoxicity. The results provide clues regarding how the body maintains a balance after exposure to environmental PP toxins. Additionally, the toxicity and side effects of WY-14643 used for the treatment of metabolic disorders might be alleviated through inducing miR-181a-5p expression.

RESULTS

P*parα* Agonists Induce miR-181a2 Expression

To determine whether P*parα* regulates miR-181a2 gene expression, HepG2 cells were treated with high-dose P*parα*-specific agonist WY-14643, followed by quantitative real-time PCR analysis of P*parα*, Pri-miR-181a2, Pre-miR-181a2, and mature miR-181a-5p expression. As positive controls, mRNA levels of the well-characterized P*parα* target genes carnitine palmitoyltransferase 1A (C*pt1a*)[27,28] and microtubule-associated protein 1 light chain 3 alpha (L*c3a*)[17,29] were also measured. No significant difference in P*parα* expression levels was observed between WY-14643 treatment group and vehicle control group (Figure S1A). The significant upregulations of C*pt1a* (2.3-fold) (Figure 1A) and L*c3a* (1.7-fold) (Figure 1B) expression demonstrated that P*parα* was activated. After P*parα* activation, mature miR-181a-5p (2-fold) expression was induced (Figure 1C). In addition to mature miR-181a-5p, we also detected the significant induction of Pri-miR-181a2 (2.2-fold) and Pre-miR-181a2 (2-fold) in response to WY-14643 treatment in HepG2 cells (Figures 1D and 1E). These data suggest that WY-14643 treatment induces miR-181a2 upregulation at the transcriptional level. Similar rises of Pri-miR-181b2 and Pre-miR-181b2 were observed in WY-14643-treated HepG2 (Figures S1B and S1C). However, the qPCR assay result of miR-181a2 host gene (miR-181a2hg) showed that P*parα* activation had no effect on miR-181a2hg (Figure S1D). It suggests that miR-181a2 and miR-181b2 may be independent transcripts from miR-181a2hg. 18*srRNA* expression was normalized to β-*actin* to confirm that template amounts are equivalent from control group and WY-14643-treated group (Figure S1E). Treatment with another synthetic highly specific P*parα* agonist, GW7647, led to a 2.2-fold induction of C*pt1a* mRNA (Figure 1G) and a 1.5-fold induction of mature miR-181a-5p expression (Figure 1F). These data further indicate that P*parα* activation induced miR-181a-5p expression.

P*parα* Enhances the Transcriptional Activity of the Hsa-miR-181a2 Promoter

To clarify whether P*parα* regulates Hsa-miR-181a2 at transcriptional level, luciferase reporter assays were performed. The putative PPRE in Hsa-miR-181a2 promoter region was predicted using an online algorithm (NUBIScan, http://www.nubiscan.unibas.ch/) (Figure 2A). Based on the finding of the prediction, luciferase reporters (pGL3-DR3-WT) containing PPRE(DR3) or mutated DR3(pGL3-DR3-Mut)were constructed and separately transfected into HepG2 cells with the Renilla luciferase expression vector pRL-TK for luciferase assays. As shown in Figure 2B, the luciferase activity of WY-14643-treated pGL3-DR3-WT group was much higher than vehicle-treated pGL3-DR3-WT group, suggesting that this region may harbor a P*parα* regulatory element. The mutation of DR3 within the construct pGL3-DR3 abolished the WY-14643-induced luciferase activity, indicating that Hsa-miR-181a2 may be directly regulated by P*parα* activation that converges on the DR3 acting as an enhancer within Pre-miR-181a2.

The direct interaction of P*parα* with the DR3 element was further substantiated by electrophoretic mobility shift assay (EMSA). The sequences of DR3 and Mut DR3 probes are shown in Figure 2C. EMSA revealed that the interaction of labeled DR3 probe with the nuclear extracts of HepG2 cells yielded a DNA/protein shift band of the expected mobility. This binding was specific because it was competitively inhibited by the addition of excess unlabeled (cold) DR3 probe, but not cold Mut DR3 probe (Figure 2D). To further verify that P*parα* binds to the enhancer DR3, we performed ChIP assays on soluble formaldehyde-cross-linked chromatin isolated from WY-14643-treated HepG2 with a monoclonal anti-P*parα* antibody. As shown in Figure 2E, the anti-P*parα* antibody precipitated the DNA fragment containing the DR3 element. Together, these results demonstrate that miR-181a2 is upregulated by P*parα* activation through binding to the DR3 element.

P*parα* Is a Direct Target of miR-181a-5p

Bioinformatic analysis was performed to search potential target genes of miR-181a-5p. We selected potential target genes from Targetscan (http://www.targetscan.org/), miRanda (http://www.microrna.org/), and PicTar (http://pictar.mdc-berlin.de/). Interestingly, among the hundreds of predicted targets, P*parα* is a potential miR-181a-5p target. Figure 3A displays the predicted miR-181a-5p-binding sites in the 3′ UTR of P*parα*. These results were further validated in 293A cells using luciferase reporter assay. The target sequence of P*parα* 3′ UTR (Figure 3B, WT) or the site-mutated sequence (Figure 3B, Mut) was cloned into the luciferase reporter vector PsiCHECK2. Next, the wild-type (WT) or mutant (Mut) vector was co-transfected with miR-181a-5p mimic or negative control mimic into 293A cells. For the P*parα* WT vector, significant repression of luciferase activity was induced by co-transfection with miR-181a-5p mimic compared with the negative control mimic co-transfection; however, for the P*parα* Mut vector, the repression of luciferase activity was abolished (Figure 3C).

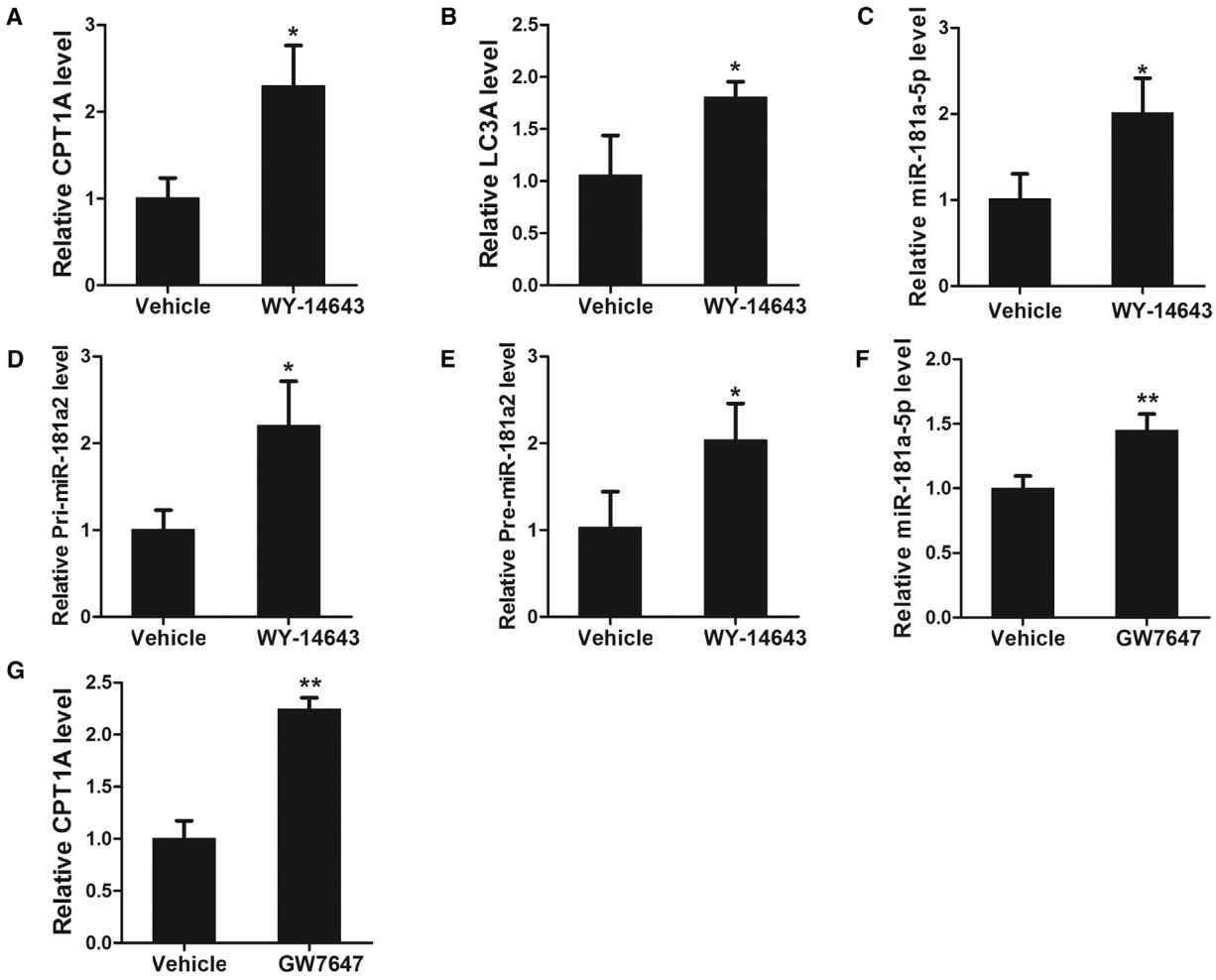

Figure 1. P*parα* Agonists Induce miR-181a2 Expression

(A and B) HepG2 cells were treated with WY-14643 (200 μM) or vehicle DMSO for 24 hr, and then the expression of C*pt1a* (A) and L*c3a* (B) was examined by quantitative real-time PCR. (C–E) Quantitative real-time PCR results displayed that WY-14643 (200 μM)-treated HepG2 cells expressed high levels of mature miR-181a-5p (C), Pri-miR-181a2 (D), and Pre-miR-181a2 (E). (F and G) HepG2 cells were treated with GW7647 (50 μM) or vehicle DMSO for 24 hr, and then the expression of mature miR-181a-5p (F) or the known P*parα* target gene C*pt1a* (G) was assayed using quantitative real-time PCR. B-*actin* was used as an internal control for the examination of C*pt1a*, L*c3a*, pri-miR-181a2, and pre-miR-181a2, while U6 snRNA was used as an internal control for the detection of mature miR-181a-5p. Data are presented as means ± SDs. *$p < 0.05$, **$p < 0.01$, determined by ANOVA.

Using western analyses, we found that P*parα* protein expression levels were significantly reduced by miR-181a-5p transfection in hepatic cell line LO2, human liver stellate cell line LX2, hepatocellular carcinoma cell lines Huh7, and HepG2 cells (Figure 3D). Exogenous P*parα* expression vector was used to verify the specificity of P*parα* antibody (the far left two bands) in HepG2 cells (Figure 3D). Altogether, these data indicate that P*parα* is a critical functional target of miR-181a-5p.

Overactivation of P*parα* Causes Cytotoxicity

Given that long-term administration of WY-14643 to mice and rats causes the carcinogenesis,[6] we then analyzed the cytotoxicity caused by high-dose WY-14643 treatment in vitro cell lines. The western blotting results displayed that the expression of P*rkcd* (known miR-181a target) was significantly decreased by induced miR-181a2 (Figure 4A); however, the expression of P*parα* had not been induced by high-dose WY-14643, which is different to previously reported moderate dose WY-14643 treatment.[12,30] The reason for the comparable P*parα* expression is that maybe it is suppressed by elevated miR-181a-5p by high-dose WY-14643 treatment (Figure 4A). Cells' exposure to overdose WY-14643 resulted in elevated ROS production in 24 hr (Figure 4B). Next, we detected whether the ROS accumulation caused by high-dose WY-14643 treatment could affect inflammatory factors expression or not. As shown in Figure 4C, the upregulation of C*yclind1* (1.5-fold) and I*l1a* (2.1-fold) were observed in high-dose WY-14643-treated HepG2 cells (Figure 4C).

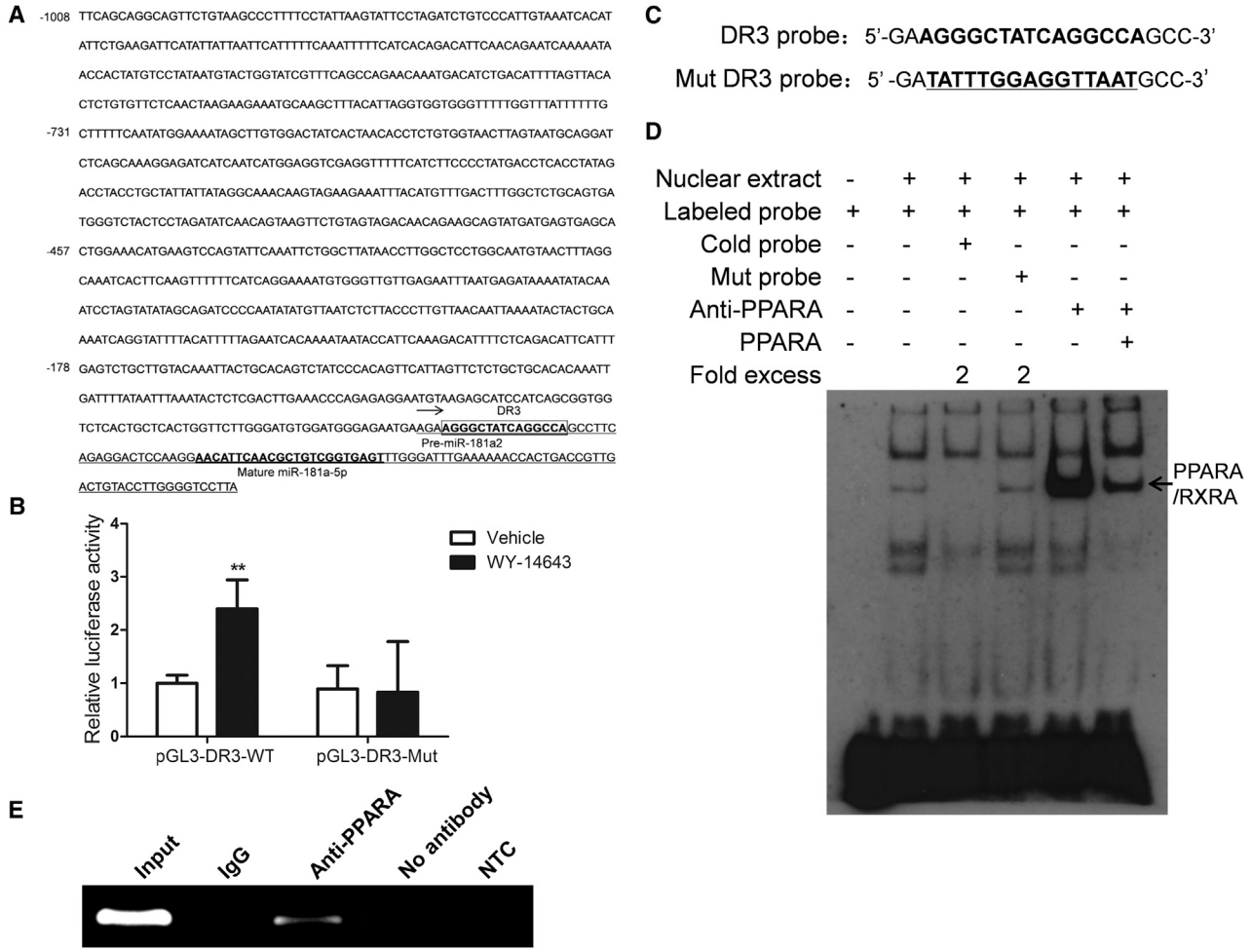

Figure 2. The Hsa-miR-181a2 Promoter Region Contains Putative PPRE in Pre-miR-181a2 and Is Directly Trans-activated by P*parα*

(A) Potential PPRE (DR3) in the Hsa-miR-181a2 promoter region was predicted using online algorithm (http://www.nubiscan.unibas.ch/). The start site of Pre-miR-181a2 is indicated by an arrow, and the PPRE/DR3 is framed. (B) PGL3-DR3-WT (containing the wild-type DR3 element) or pGL3-DR3-Mut (containing the mutant DR3 element) was co-transfected into HepG2 cells with the Renilla luciferase expression vector pRL-TK. After 6 hr of incubation, the cells were treated with vehicle DMSO or 200 μM WY-14643 for 36 hr, and then dual-luciferase assays were performed. Firefly luciferase activity was normalized to that of Renilla luciferase. The data are shown as means ± SDs, *$p < 0.05$, **$p < 0.01$, determined by ANOVA. (C) The sequences of the DR3 probe and mutant DR3 probe are shown. The DR3 element is in bold, and the mutated bases are underlined. (D) EMSA analysis of the binding of HepG2 cell nuclear proteins to the DR3 was performed. The position of the shifted P*parα*/R*xrα* complex is indicated. (E) ChIP assays were performed using chromatin isolated from WY-14643-treated HepG2 cells. Anti-P*parα* was used for immunoprecipitation of the chromatin DNA fragment, taking IgG as a negative control. The precipitated DNA was extracted and amplified by PCR using primers spanning the DR3 element. The input (total DNA extract) was used as positive PCR control. No antibody (no anti-P*parα* and IgG in the reaction) was used as mock control. The ultrapure water was used instead of the template as no template control (NTC).

However, the inflammatory factor I*l6* expression had not been affected by high-dose WY-14643 exposure, which may be the pathways that regulates I*l6* is different from that regulates I*l1a* and C*yclind1* (data not shown).

To examine the effects of high-dose WY-14643 on DNA damage, the phosphorylated form of histone H*2a.x* Ser 139 (γ-H*2a.x*), as a specific biomarker of DNA double-strand breaks (DSBs), was detected by immunoblot assay. High-dose WY-14643 treatment caused a clear increased DSBs, as indicated by increased γ-H*2a.x* in WY-14643-treated HepG2 cells relative to vehicle control, accompanied with the increased DSBs, the central homologous recombination repair protein, R*ad51* expression was significantly induced (Figure 4D).

TUNEL assay was performed to assess the effects of high-dose WY-14643 on cell apoptosis. As shown in Figure 4E, the number of apoptotic HepG2 cells was significantly increased after overdose WY-14643 treatment. These results of ROS, DNA damage, inflammatory factor expression, and apoptosis directly demonstrate that P*parα* overactivation causes cytotoxicity.

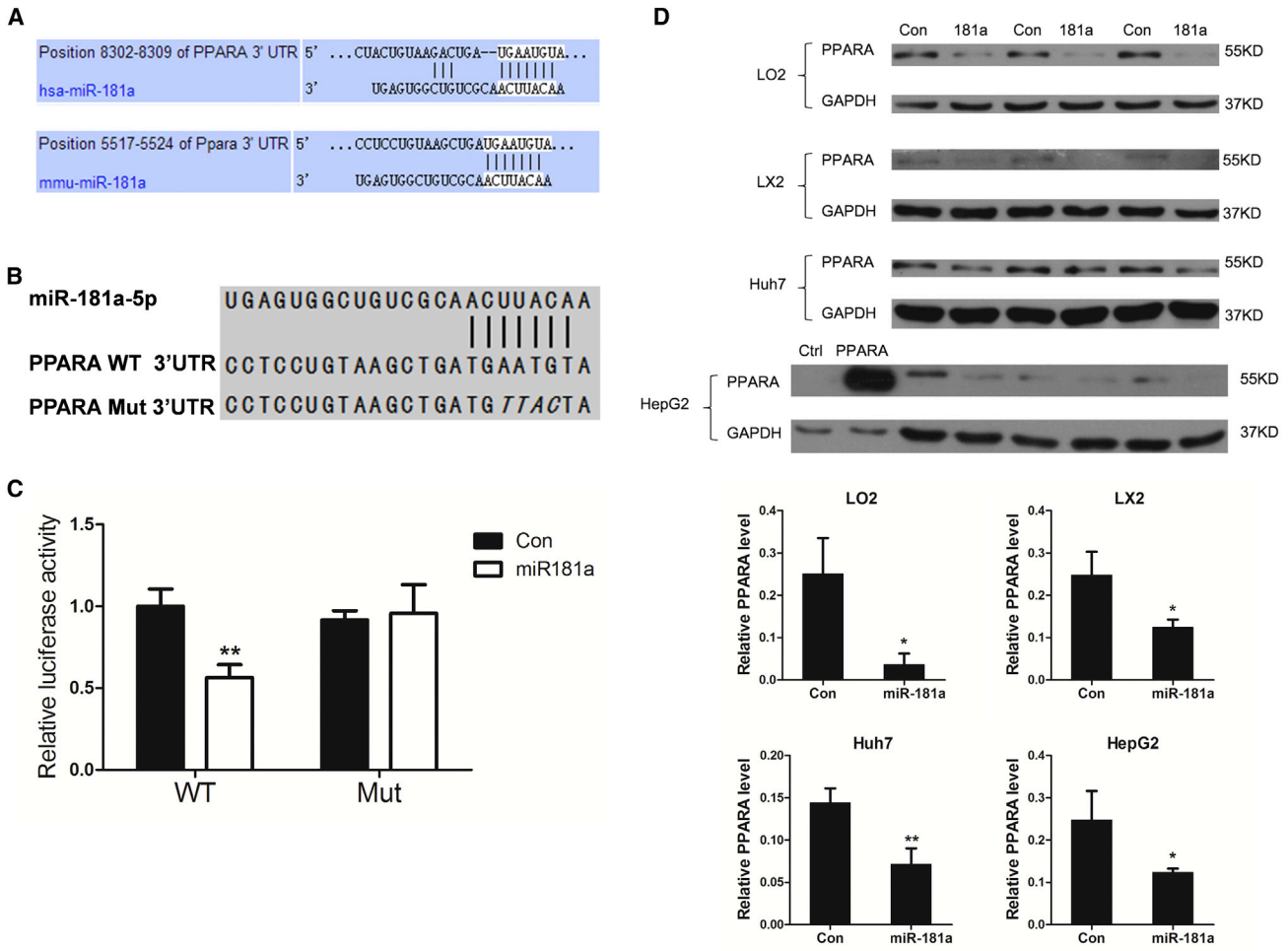

Figure 3. miR-181a-5p Target Gene Prediction, Verification, and the Regulation of miR-181a-5p on P*parα*

(A) The seed sequence base pairing between miR-181a-5p and the 3′ UTRs of P*parα* was predicted by TargetScan (http://www.targetscan.org/), miRanda (http://www.microrna.org/) and PicTar (http://pictar.mdc-berlin.de/). (B) Sketch of the construction of wild-type (WT) or mutant (Mut) P*parα* 3′UTR vectors, where the mutant binding sequences are italicized. (C) Relative luciferase activity assays of luciferase reporters with wild-type or mutant P*parα* 3′ UTR were performed after co-transfection with the miR-181a-5p (miR181a) mimic or control (Con) mimic. PsiCHECK 2-3′ UTR reporter plasmid in which the luciferase coding sequence had been fused to the 3′ UTR of P*parα* was co-transfected into 293A cells with the control mimic or miR-181a-5p mimic. Renilla luciferase activity was normalized to that of Firefly luciferase. The 3′ UTR-Mut indicates the introduction of alterations into the seed complementary sites shown in (B). (D) LO2, LX2, Huh7, or HepG2 cells were transiently transfected with control mimic or miR-181a-5p mimic in vitro. Forty-eight hours later, cells were collected, and the protein level of P*parα* was detected by western blotting (upper) and calculated by ImageJ (lower). G*apdh* was used as loading control. HepG2 cells were transfected with P*parα* expression construct or a control vector to verify the specificity of P*parα* antibody (the far left two bands). The data are shown as means ± SDs. *p < 0.05, **p < 0.01, determined by ANOVA.

Exogenous Expression miR-181a-5p Attenuates the Cytotoxicity Caused by P*parα* Overactivation

Since P*parα* overactivation causes varied cytotoxic effects and miR-181a-5p can suppress P*parα* at a post-transcriptional level, we then detected whether exogenous expression miR-181a-5p could alleviate the cytotoxicity caused by P*parα* overactivation or not.

HepG2 cells or LO2 cells were transfected with miR-181a-5p mimic or control mimic for 6 hr and then were treated with high concentrations of WY-14643 for 48 hr; the protein expression of miR-181a-5p targets P*parα* and P*rkcd* was analyzed by western blotting (Figure 5A). As illustrated in Figure 5A, P*parα* and P*rkcd* were significantly reduced in miR-181a-5p mimic transfection group compared to the control. Also, as indicated in Figure 5B, exogenous expression of miR-181a-5p reduced the ROS level caused by overactivated P*parα*. Next, we detected if exogenous expression of miR-181a-5p could affect inflammatory factors I*l1a* and C*yclind1* expression. HepG2 cells were transfected with miR-181a-5p mimic or control mimic for 6 hr and then were treated with high concentrations of WY-14643 for 48 hr. Quantitative real-time PCR analysis showed that C*yclind1*

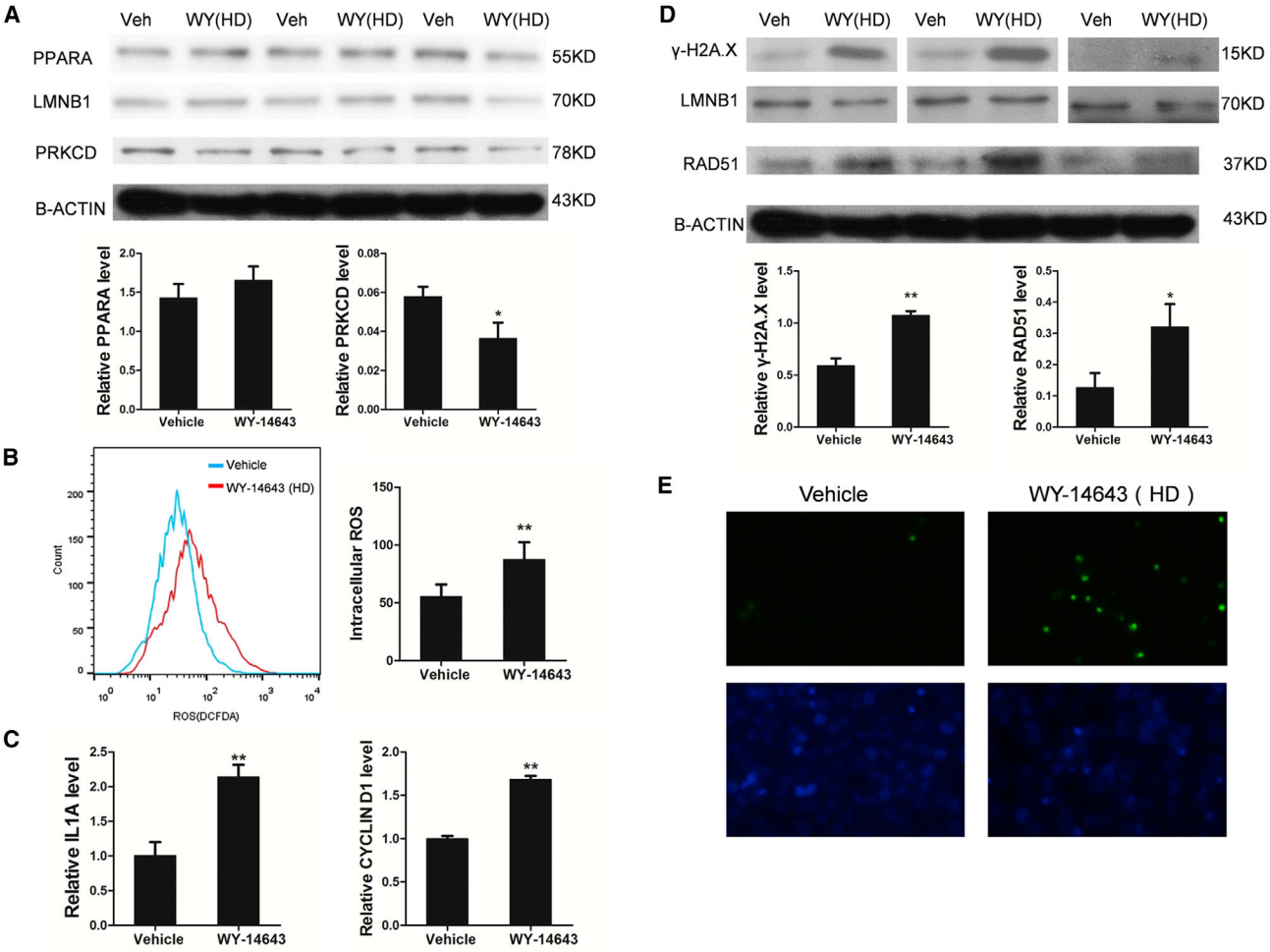

Figure 4. Overactivated P*parα* Causes Cytotoxicity

(A) HepG2 cells and LO2 cells was treated with a high dose (HD) of WY-14643 (400 μM) or vehicle (Veh) DMSO for 48 hr, and then the protein levels of P*parα* and L*mnb1* from HepG2 cells nuclear protein or P*rkcd* and β-*actin* from LO2 cells lysate were detected by western blotting (upper) and calculated by ImageJ (lower). (B) HepG2 cells were treated with a high concentration of WY-14643 (400 μM) or vehicle DMSO for 24 hr, and then flow cytometry was performed to analyze the ROS levels in HepG2 cells. Left, representative flow cytometry analysis showing the intensities of ROS (CM-H2DCFDA) in HepG2 cells. Right, histogram summarizes the ROS levels in HepG2 cells. (C) HepG2 cells were treated with a high concentration of WY-14643 (400 μM) or vehicle DMSO for 48 hr, and then the expression levels of C*yclind1* and I*l1a* were assayed using quantitative real-time PCR. (D) LO2 cells and HepG2 cells were treated with a high concentration of WY-14643 (400 μM) or vehicle DMSO for 48 hr, and then cells were collected. The protein expression of R*ad51* and γ-H*2a.x* were measured by western blotting (upper) and calculated by ImageJ (lower); the increased R*ad51* protein expression and γ-H*2a.x* were observed in WY-14643-treated LO2 cells and HepG2 cells, respectively. B-actin was used as an internal control for the examination of R*ad51*, while L*mnb1* was used as an internal control for the detection of γ-H*2a.x*. (E) HepG2 cells were treated with a high concentration of WY-14643 (400 μM) or vehicle DMSO for 48 hr, and then cells were subjected to the TUNEL assay. The data are shown as means ± SDs, *$p < 0.05$, **$p < 0.01$, determined by ANOVA.

and I*l1a* mRNA levels were decreased in exogenous of miR-181a-5p treatment group (Figure 5C).

The effect of exogenous expression miR-181a-5p on DNA damage caused by P*parα* overactivation was examined, too. Exogenous expression of miR-181a-5p significantly reduced γ-H*2a.x* level that was due to overactivated P*parα* (Figure 5D). R*ad51* expression induced by high-dose WY-14643 was obviously alleviated by the exogenous expression miR-181a-5p (Figure 5D). The TUNEL assay showed decreased numbers of TUNEL-positive HepG2 cells after the overexpression of miR-181a-5p (Figure 5E). All these results demonstrated that exogenous expression of miR-181a-5p dramatically attenuated the cytotoxicity caused by P*parα* overactivation.

DISCUSSION

Recently, the potential significance of miRNAs in the process of carcinogenesis caused by long-term exposure of WY-14643 to mice has been highlighted by accumulating studies.[14,31,32] Here, we found that short-term exposure of HepG2 cells to high-dose P*parα*-specific agonist WY-14643-induced miR-181a-5p expression may play a

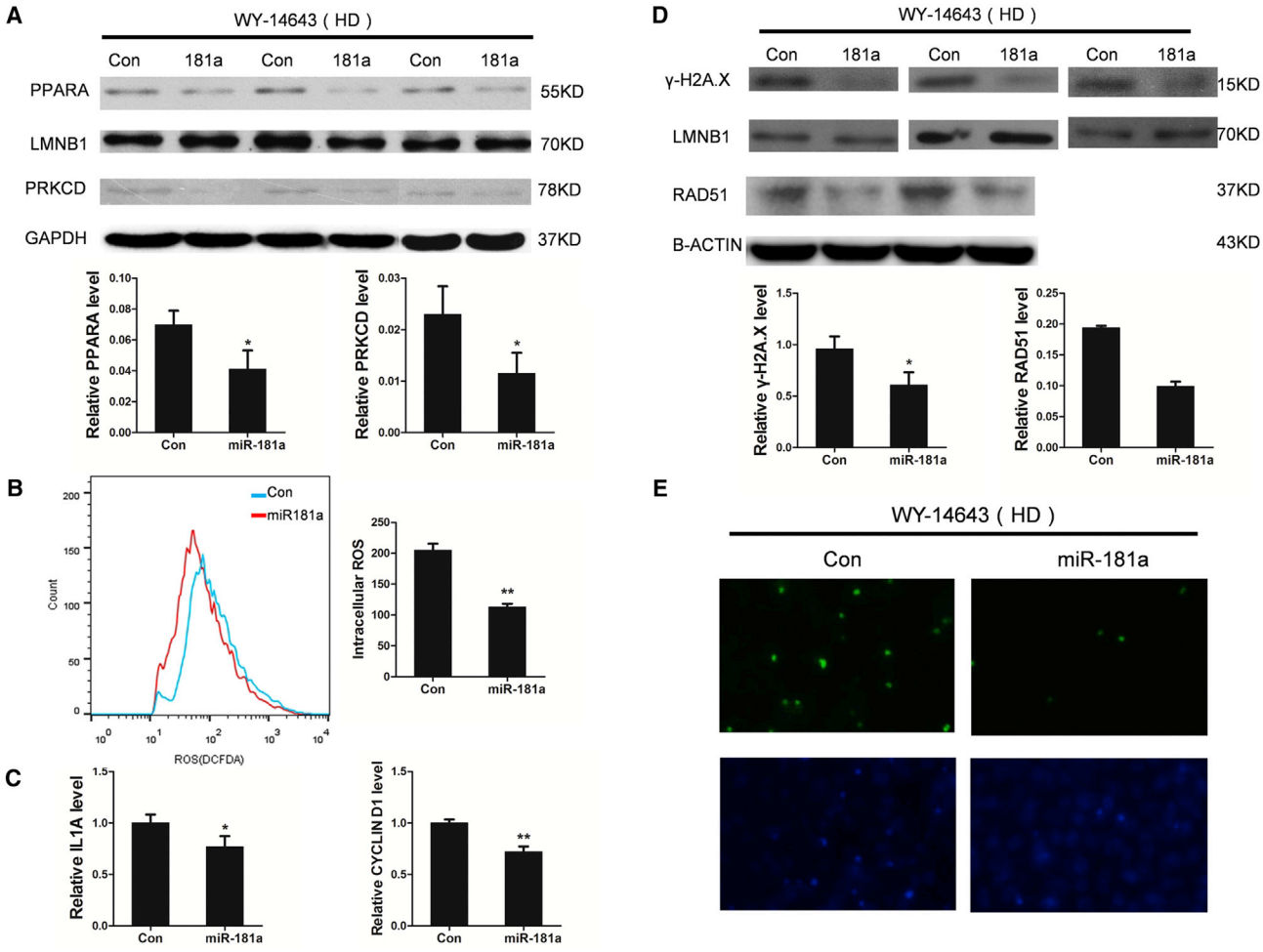

Figure 5. Exogenous Expression of miR-181a-5p Reduces the Cytotoxicity Induced by P*parα* Overactivation

(A) HepG2 cells and LO2 cells were transfected with the miR-181a-5p mimic or control mimic for 6 hr and then were treated with a high concentration of WY-14643 (400 μM) for 48 hr, and then the protein levels of P*parα* and L*mnb1* from HepG2 cells nuclear protein and P*rkcd* and G*apdh* from LO2 cells lysate were detected by western blotting (upper) and calculated by ImageJ (lower). (B) HepG2 cells were transfected with the miR-181a-5p mimic or control mimic for 6 hr and then treated with a high concentration of WY-14643 (400 μM) for 24 hr, followed by flow cytometry analysis of the ROS levels in HepG2 cells. Left, representative flow cytometry analysis showing the intensities of ROS (CM-H2DCFDA) in HepG2 cells. Right, histogram summarizes the ROS levels in HepG2 cells. (C) HepG2 cells were transfected with the miR-181a-5p mimic or control mimic for 6 hr and then were treated with a high concentration of WY-14643 (400 μM) for 48 hr, followed by assay of the expression of C*yclind1* and I*l1a* using quantitative real-time PCR. (D) LO2 cells and HepG2 cells were transfected with the miR-181a-5p mimic or control mimic for 6 hr and then were treated with a high concentration of WY-14643 (400 μM) for 48 hr, and then cells were collected. The protein expression of R*ad51* and γ-H*2a.x* were measured by western blotting (upper) and calculated by ImageJ (lower); the decreased R*ad51* protein expression and γ-H*2a.x* were observed in WY-14643-treated LO2 cells and HepG2 cells, respectively. B-actin was used as an internal control for the examination of R*ad51*, while L*mnb1* was used as an internal control for the detection of γ-H*2a.x*. (E) HepG2 cells were transfected with the miR-181a-5p mimic or control mimic for 6 hr and then were treated with a high concentration of WY-14643 (400 μM) for 48 hr, and then cells were subjected to the TUNEL assay. The data are shown as means ± SDs, *$p < 0.05$, **$p < 0.01$, determined by ANOVA.

crucial role in balancing the cytotoxic effects caused by P*parα* overactivation.

The NR P*parα*, a multi-functional transcription factor, has received numerous attentions as a therapeutic target for its lipid-lowering action.[33–35] Normally, P*parα* is moderately activated and participates in a diverse range of biological functions, including control of fatty acid transport and catabolism, atherosclerosis, oxidative stress, anti-inflammation, immunomodulation, and autophagy.[11,17,36–38] Previous studies demonstrated that P*parα* can sequester the p65 subunit of the N*fκb* complex and prevent N*fκb*-dependent regulation of genes involved in pro-inflammatory responses.[39,40] However, cardiac-specific overexpression of P*parα* in mice contributes to the development of cardiac dysfunction. It is partially because of the generation of ROS produced by increased mitochondrial flux.[19] Excessive production of ROS may inflict various biological responses, ranging from a transient

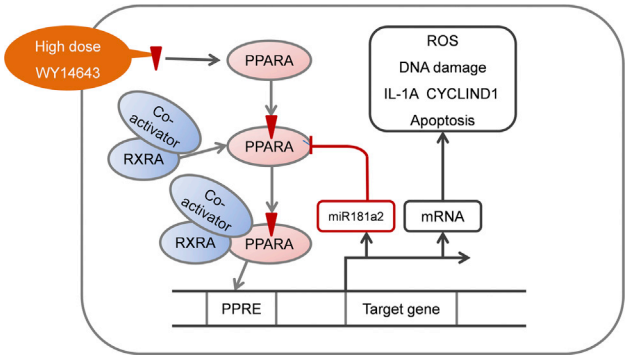

Figure 6. A Summary Schematic of P*parα* and miR-181a2

The diagram shows the effects of WY-14643, miR-181a2, and P*parα* on cytotoxicity caused by P*parα* overactivation. WY-14643 enhanced the expression of miR-181a2, and miR-181a-5p targeted P*parα* and repressed its expression and then reduced cytotoxicity caused by P*parα* overactivation.

growth arrest, permanent growth arrest or senescence, apoptosis, and necrosis.[41] It has been reported that higher levels of ROS can induce I*l1a* secretion in macrophages from A*tg5*$^{-/-}$ mice.[42] We found that high-dose WY-14643 treatment induced significantly elevated ROS production, and increased expression of inflammatory factors C*yclind1* and I*l1a* was observed. The elevated ROS levels caused by P*parα* overactivation may be the major role that induces I*l1a* and C*yclind1* expression in high-dose WY-14643-treated HepG2 cells. Cytotoxicity always elicits an inflammatory response, too.[43] Damage caused by ROS is considered the most common type of DNA lesion.[41] Our results showed that P*parα* overactivation induced DNA damage and the central homologous recombination repair protein R*ad51* expression. Distinct roles of P*parα* have been reported in regulating apoptosis depending on cell types, ligand types, ligands dose, et al. P*parα* antagonist NXT629 can induce apoptosis and inhibit proliferation of chronic lymphocytic leukemia cells in vitro and in vivo.[44] P*parα* agonist fenofibrate inhibits aldosterone-induced apoptosis in adult rat ventricular myocytes via stress-activated kinase-dependent mechanisms.[45] However, P*parα* activators can also induce apoptosis in activated macrophages and then contribute to the treatment of atherosclerosis.[16] P*parα* serves an E3 ubiquitin ligase to induce B*cl2* ubiquitination and degradation leading to cell apoptosis in response to chemotherapy drugs.[46] P*parα* agonist fenofibrate induces effective apoptosis in mantle cell lymphoma by inhibiting the T*nfα*/N*fκb* signaling axis.[47] Here, we found that P*parα* overactivation can significantly induces cells apoptosis .

Accumulating evidence suggests that transcription factors can bind to the promoters or enhancers of miRNAs and regulate their expression. Previous reports demonstrated that 27 miRNAs were significantly regulated following WY-14643 treatment.[14] These implied that miRNA dysregulation caused by WY-14643-induced P*parα* activation may play a pivotal role in P*parα* agonist-induced cytotoxic effects. It has been widely reported that miR-181a expression is frequently regulated by genotoxic agent treatment. Stimulation with genotoxic agents, such as chemotherapeutic drugs doxorubicin or cisplatin, was found to induce miR-181a expression in breast cancer cells or non-small-cell lung cancer A549 cells.[25,48] Our results revealed that P*parα*-specific agonist WY-14643 can induce miR-181a2 expression accompanied by the induction of miR-181b2, but not miR-181a2hg. A previous report demonstrated that ~35% of intronic miRNAs are independent of host gene transcription,[49] and miR-181a2 and miR-181b2 may be independent transcription from miR-181a2hg. The reported miR-181a1 promoter lies in upstream region of Pre-miR-181a1, not miR-181a1hg.[25,50] Therefore, the promoter of miR-181a2 is more likely located in the upstream region of Pre-miR-181a2, not miR-181a2hg. NUBIScan prediction and luciferase reporter assay results found a DR3 located in pre-miR-181a2, but not in mature miR-181a2. Previous reports revealed that a large fraction of transcription factor (TF)-binding sites of miRNAs lie close to the pre-miRNAs, and some TF-binding sites located in downstream regions may represent some distal regulatory elements (enhancers or silencers).[51] Therefore, PPRE(DR3) located in pre-miR-181a2 may be an enhancer of pre-miR-181a2. Our EMSA and chromatin immunoprecipitation (ChIP) assay results verified that P*parα* directly binds to the DR3 and regulates miR-181a2 expression. Then the increased miR-181a-5p can in turn repress its reported target P*rkcd* expression.[52] Decreased P*rkcd* level may partially inhibit apoptosis, but the final outcome of P*parα* overactivation is to promote apoptosis.

The miR-181 family plays diverse roles in regulating key aspects of cellular growth, development, inflammatory response, differentiation, and autophagy.[24,25,53–56] Bioinformatic analysis and our results indicated that miR-181a-5p targets P*parα*. We found that the intracellular DNA damage and apoptosis induced by overdose WY-14643 treatment were significantly reduced by the ectopic expression of miR-181a-5p. Our results displayed that exogenous expression of miR-181a-5p significantly reduced the intracellular ROS level, and inflammatory factors I*l1a* and C*yclind1* levels caused by P*parα* overactivation. It is anticipated that suppression of P*parα* signaling can decrease the cytotoxic effects caused by a high concentration of WY-14643. A feedback loop regulation between miR-181a-5p and P*parα* was revealed by our experiments.

As we know, PPs are widely distributed in the environment. It is inevitable for human to contact with known or unknown PPs. Previously, extensive studies focused on the risk put to human by exposure to these components. However, the body comes into contact with the PP toxic substances in the environment frequently. Thus, how does the body reduce harm to itself to keep healthy, and by which mechanism? Our experiments show that the feedback loop regulation between miR-181a-5p and P*parα* plays an important role in facilitating a balance in the cytotoxicity caused by high concentrations of WY-14643 (Figure 6). Inducible miR-181a2 by P*parα* overactivation plays critical roles in this protective process, and the induced miR-181a-5p depressed the excess P*parα* levels. Such a balancing mechanism would assist the establishment of meaningful human

risk assessments and also aid the rational design of improved drugs. It should also be noted that there are many potential targets of miR-181a-5p that could also contribute to the effect. Further studies are needed to provide a comprehensive picture to understand the miR-181a-5p alleviation of the toxic effects caused by high concentration of WY-14643.

MATERIALS AND METHODS

Reagents

The P*parα* agonists WY-14643 and GW7647 were purchased from Cayman Chemical Company (Michigan, USA). For ex vivo experiments, WY-14643 and GW7647 were dissolved in DMSO at 0.1%–0.2% final concentration. The PrimeScript RT Reagent Kit with gDNA Eraser was purchased from TaKaRa, Japan. The dual luciferase assay system was from Promega (Madison, WI). The EMSA Assay kit and ChIP Assay kit were from Beyotime (Shanghai, China). Antibodies against γ-H2*a.x* (#2577s) and P*rkcd* (#9616) were from Cell Signaling Technology (Danvers, MA, USA). Antibodies against P*parα* (sc-398394), β-*actin* (sc-47778), R*ad51* (sc-398587), goat anti-rabbit immunoglobulin G-horseradish peroxidase (IgG-HRP) (sc-2004), and goat anti-mouse IgG-HRP (sc-2005) were purchased from Santa Cruz Biotechnology (CA, USA). G*apdh* antibody (BM-1623) was from Boster Biological Technology (Wuhan, China). L*mnb1* antibody (A1910) was purchased from ABclonal (MA, USA).

Cell Culture and miRNA Transfection

The cell lines HepG2, 293A, LX2, Huh7, and LO2 were cultured in DMEM (Life Technologies, Carlsbad, USA) with 10% fetal bovine serum (FBS), streptomycin (100 U/mL), and penicillin (100 U/mL) at 37°C in a 5% CO_2 humid incubator. miRNA mimics were transfected at a concentration of 40 nM using RNAimax (Invitrogen, Carlsbad, USA) according to the manufacturer's instructions. The mimic sequences sets for miRNA transfection are listed in Table S1.

Quantitative Real-Time PCR

A specific stem loop primer was utilized for the reverse transcription of mature miR-181a-5p. For examination of the miRNA and mRNAs, total RNA was extracted with Trizol reagent (TaKaRa, Japan), and then the first-strand cDNA was synthesized using the PrimeScript RT Reagent Kit with gDNA Eraser (TaKaRa, Japan). Real-time PCR was performed using the SYBR Green Real-Time PCR Master Mix (Toyobo, Japan). The relative levels of the mRNAs were normalized to that of β-*actin* mRNA. The relative levels of the miRNA were normalized to that of U6 small nuclear RNA (snRNA). Relative expression of these genes was calculated using the $^{\Delta\Delta}$CT method. The primer sets for quantitative real-time PCR are listed in Table S2.

Western Blotting

Nuclear extracts were prepared using the Active Motif Nuclear Extract Kit (catalog nos. 40010 and 40410) according to the manufacturer's instructions. Cells were lysed in radioimmunoprecipitation assay (RIPA) buffer according to the manufacturer's instructions (Beyotime, Jiangsu, China) to prepare whole-protein extracts. Protein lysates were separated by 10% or 12% SDS-PAGE (20 μg each lane). Next, the gel was transferred to polyvinylidene fluoride (PVDF) membranes (Millipore, USA). After blocking with 5% skimmed milk or 5% BSA in Tris-buffered saline/Tween-20 (TBST), the membranes were incubated with the primary antibodies overnight at 4°C, and then with the respective HRP-conjugated secondary antibodies at room temperature for 1.5 hr. Finally, the membranes were visualized with enhanced chemiluminescence (ECL) (Bio-Rad, USA). The signal was analyzed by ImageJ. Each experiment was performed in triplicate except for Figure 5D R*ad51*.

Plasmid Construction, Transfection, and Luciferase Reporter Assay

Putative PPREs in the Hsa-miR-181a2 promoter region were predicted using an online algorithm (NUBIScan: http://www.nubiscan.unibas.ch/). Based on this prediction (Figure 2A), the Hsa-miR-181a2 promoter region was amplified by PCR using LO2 cell genomic DNA as a template (the primer sequences are listed in Table S3). The fragments were then separately inserted between the KpnI and XholI sites of the pGL3-basic vector (Promega, USA), and the resulting plasmids were named as follows with the fragment of the Hsa-miR-181a2 promoter region specified: pGL3-DR3(−319 to +105) (also named pGL3-DR3-WT); pGL3- DR3-Mut, derived from pGL3-DR3-WT, contained mutations in the DR3 element (AGGGCTATCAGGCCA; the mutated bases are underlined). For luciferase reporter assays, the above plasmids were separately co-transfected with the Renilla luciferase expression vector pRL-TK (Promega, USA) into HepG2 cells using Lipofectamine 2000 (Invitrogen, Carlsbad, USA) according to the manufacturer's protocol. After 6 hr of incubation, the cells were treated with vehicle DMSO or WY-14643 (200 μM) for 36 hr. The cells were then harvested for detection of luciferase activity using the dual-luciferase assay kit (Promega, USA) according to the manufacturer' s instructions. The enzymatic activity of luciferase was measured using a Fluoroskan Ascent FL (Thermo Scientific, USA). Firefly luciferase activity was normalized to that of Renilla luciferase activity.

PsiCHECK-2 vectors containing WT or mutated miR-181a-5p Mut response elements (MREs) from the P*parα* 3′ UTR were co-transfected with miR-181a-5p mimic or control mimic into 293A cells. Forty-eight hours later, cells were lysed. Firefly and Renilla luciferase activities were measured using a dual-luciferase reporter assay system (Promega, USA). The results were normalized Renilla luciferase activity to that of Firefly luciferase activity.

Plasmids of PcDNA3.1 or PcDNA3.1-P*parα* from Lisheng Zhang's laboratory were transfected with lipofectamine 2000 into HepG2 cells according to the manufacturer's protocol.

EMSA

Nuclear extracts were prepared from WY-14643-treated HepG2 cells with or without exogenous expression P*parα* using the Active Motif Nuclear Extract Kit (Active Motif, CA, USA, nos. 40010 and 40410), and the protein concentrations were determined using the BCA protein assay kit (Beyotime, Jiangsu, China). Double-stranded

oligonucleotides (Sangon, Shanghai, China) corresponding to the DR3 within the Hsa-miR-181a2 promoter were synthesized and annealed into double strands. The DNA binding activity of P*parα* was detected by a chemiluminescent EMSA Kit. The binding reactions were performed separately in a 10 μL reaction mixture containing 5× gel shift binding buffer and 10 μg of nuclear proteins. For supershift assays, 1 μL of antibody against P*parα* (Santa Cruz, CA, USA, sc-398394) was mixed with nuclear proteins in supershift assay and exogenous expression P*parα* assay and incubated on 25°C for 20 min. For competition experiments, unlabeled (cold) DR3 or Mut DR3 probe was added to the reaction mixture at 2× excess concentrations over the labeled probe. The mixtures were then incubated at room temperature for 10 min. Subsequently, 5 pmol of labeled probe was added to each reaction mixture and incubated at room temperature for 10 min. All of the reaction products were analyzed by electrophoresis in a 6.6% non-denaturing polyacrylamide gel in 0.5× Tris-borate-EDTA. The nylon was visualized using ECL (Bio-Rad, USA). The DNA-binding reaction system and double-stranded oligonucleotides are listed in Table S4 and Figure 2C, respectively. The reactions were analyzed by electrophoresis in a non-denaturing 6.6% polyacrylamide gel, followed by development.

ChIP

ChIP assays were performed using the ChIP Assay kit (Beyotime, Jiangsu, China) according to the manufacturer's instructions. In brief, HepG2 cells were treated with 200 μM WY-14643 for 24 hr, and then incubated with formaldehyde at a final concentration of 1% (v/v) for 10 min at 37°C to cross-link the nuclear proteins to DNA. Subsequently, cells were sonicated and then immunoprecipitated with the antibody against P*parα*, taking IgG as a negative control and no antibody (no anti-P*parα* and IgG in the reaction) as mock control. The captured chromatin was eluted and un-cross-linked, and the DNA was recovered. The ChIP-isolated DNA was subjected to PCR amplification using the primer pair spanning the PPRE/DR3 in miR-181a2 promoter region (the primer sequences are listed in Table S2).

ROS Assay

After treatment with WY-14643 or vehicle with or without the transfection of miR-181a-5p or control mimics, the cells were resuspended in 500 μL of phosphate buffered saline, and then cells were loaded with 20 μM 2',7' -dichlorofluorescin diacetate (DCF-DA; Sigma-Aldrich, St. Louis, USA) at 37°C for 30 min. Cells were washed in 500 μL of phosphate buffered saline (PBS) three times and then resuspended again in 500 μL of phosphate buffered saline. Fluorescence was measured by a flow cytometer (FACSCalibur, BD Biosciences, USA) with an excitation at 488 nm and an emission at 525 nm. For each sample 10,000 events were collected. The mean dichlorodihydrofluorescein (DCF) fluorescence intensity were analyzed with FlowJo software.

TUNEL Assay

TUNEL assays were performed according to the manufacturer's instructions (Roche, Basel, Switzerland). In brief, after treatment with WY-14643 or vehicle with or without transfection of miR-181a-5p or control mimics, cells were washed three times in PBS and were fixed in freshly prepared 4% paraformaldehyde in PBS for 1 hr at room temperature, followed by washing with PBS and permeabilization in 0.1% Triton X-100 in 0.1% sodium citrate. Cells were then incubated with TUNEL reaction mixture (Roche) for 60 min at 37°C in a humidified atmosphere in the dark. After washing twice with PBS, the cells were counterstained by DAPI (Beyotime, Jiangsu, China) and evaluated by fluorescence microscopy.

Statistical Analysis

All experiments (except for Figure 5D R*ad51*) were performed in triplicate or higher. Statistical analysis was performed using ANOVA. Data were presented as the means ± SDs, and the level of statistical significance was set at $^{*}p < 0.05$, $^{**}p < 0.01$.

SUPPLEMENTAL INFORMATION

Supplemental Information includes one figure and four tables and can be found with this article online at https://doi.org/10.1016/j.omtn.2017.09.008.

AUTHOR CONTRIBUTIONS

L.Z. and G.L. conceived and designed the experiments, wrote the manuscript, and contributed to funding acquisition; Y.C. performed the experiments, analyzed the data, and wrote the manuscript. Z.W. conducted the experiments and performed statistical analyses. S.X. designed the experiments and revised the article. Y.P. conducted the experiments and revised the article. Y.Y., D.Q., and S.L. conducted the experiments. Y.X. performed statistical analyses and revised the article. All authors reviewed the manuscript.

CONFLICTS OF INTEREST

The authors declare no conflict of interest.

ACKNOWLEDGMENTS

The project is supported by the Fundamental Research Funds for the Central Universities (2662016PY087 and 2662017PY106), National Key R&D Plan No. 2017YFA0103200 and 2017YFA0103202, HZAU Startup funds to L.Z., and Inner Mongolia Autonomous Region Major Basic Research Funds to G.L. and L.Z.

REFERENCES

1. Hays, T., Rusyn, I., Burns, A.M., Kennett, M.J., Ward, J.M., Gonzalez, F.J., and Peters, J.M. (2005). Role of peroxisome proliferator-activated receptor-α (PPARalpha) in bezafibrate-induced hepatocarcinogenesis and cholestasis. Carcinogenesis *26*, 219–227.

2. Kobayashi, K., Matsuyama, W., Arai, Y., Koizumi, S., Shimizu, T., Tomioka, R., and Sasaki, K. (2016). Boiogito increases the metabolism of fatty acids in proximal tubular cells through peroxisome proliferators-activated receptor (PPAR) α agonistic activity. Biol. Pharm. Bull. *39*, 143–147.

3. Klaunig, J.E., Babich, M.A., Baetcke, K.P., Cook, J.C., Corton, J.C., David, R.M., DeLuca, J.G., Lai, D.Y., McKee, R.H., Peters, J.M., et al. (2003). PPARalpha agonist-induced rodent tumors: modes of action and human relevance. Crit. Rev. Toxicol. *33*, 655–780.

4. Peters, J.M., Cattley, R.C., and Gonzalez, F.J. (1997). Role of PPAR alpha in the mechanism of action of the nongenotoxic carcinogen and peroxisome proliferator Wy-14,643. Carcinogenesis *18*, 2029–2033.

5. Patterson, A.D., Shah, Y.M., Matsubara, T., Krausz, K.W., and Gonzalez, F.J. (2012). PPARα-dependent induction of uncoupling protein 2 protects against acetaminophen-induced liver toxicity. Hepatology *56*, 281–290.

6. Woods, C.G., Burns, A.M., Bradford, B.U., Ross, P.K., Kosyk, O., Swenberg, J.A., Cunningham, M.L., and Rusyn, I. (2007). WY-14,643 induced cell proliferation and oxidative stress in mouse liver are independent of NADPH oxidase. Toxicol. Sci. *98*, 366–374.

7. Du, W.W., Liu, F., Shan, S.W., Ma, X.C., Gupta, S., Jin, T., Spaner, D., Krylov, S.N., Zhang, Y., Ling, W., and Yang, B.B. (2015). Inhibition of Dexamethasone-induced fatty liver development by reducing miR-17-5p levels. Mol. Ther. *23*, 1222–1233.

8. Zhi, X., Zhou, X.E., Melcher, K., and Xu, H.E. (2016). Structures and regulation of non-X orphan nuclear receptors: a retinoid hypothesis. J. Steroid Biochem. Mol. Biol. *157*, 27–40.

9. Carter, E.L., Gupta, N., and Ragsdale, S.W. (2016). High affinity Heme binding to a Heme regulatory motif on the nuclear receptor Rev-erbβ leads to its degradation and indirectly regulates its interaction with nuclear receptor corepressor. J. Biol. Chem. *291*, 2196–2222.

10. Steffensen, K.R. (2015). Are synthetic compounds that silence the liver-x-receptor the next generation of anti-cancer drugs? Cancer Cell *28*, 3–4.

11. Roy, A., Kundu, M., Jana, M., Mishra, R.K., Yung, Y., Luan, C.-H., Gonzalez, F.J., and Pahan, K. (2016). Identification and characterization of PPARα ligands in the hippocampus. Nat. Chem. Biol. *12*, 1075–1083.

12. Kim, J.-H., Qu, A., Reddy, J.K., Gao, B., and Gonzalez, F.J. (2014). Hepatic oxidative stress activates the Gadd45b gene by way of degradation of the transcriptional repressor STAT3. Hepatology *59*, 695–704.

13. Tsai, F.-Y., Cheng, Y.-T., and Tsou, T.-C. (2014). A recombinant PPRE-driven luciferase bioassay for identification of potential PPAR agonists. Vitam. Horm. *94*, 427–435.

14. Shah, Y.M., Morimura, K., Yang, Q., Tanabe, T., Takagi, M., and Gonzalez, F.J. (2007). Peroxisome proliferator-activated receptor α regulates a microRNA-mediated signaling cascade responsible for hepatocellular proliferation. Mol. Cell. Biol. *27*, 4238–4247.

15. Pawlak, M., Lefebvre, P., and Staels, B. (2015). Molecular mechanism of PPARα action and its impact on lipid metabolism, inflammation and fibrosis in non-alcoholic fatty liver disease. J. Hepatol. *62*, 720–733.

16. Chinetti, G., Griglio, S., Antonucci, M., Torra, I.P., Delerive, P., Majd, Z., Fruchart, J.C., Chapman, J., Najib, J., and Staels, B. (1998). Activation of proliferator-activated receptors α and γ induces apoptosis of human monocyte-derived macrophages. J. Biol. Chem. *273*, 25573–25580.

17. Lee, J.M., Wagner, M., Xiao, R., Kim, K.H., Feng, D., Lazar, M.A., and Moore, D.D. (2014). Nutrient-sensing nuclear receptors coordinate autophagy. Nature *516*, 112–115.

18. Sengupta, S., Peterson, T.R., Laplante, M., Oh, S., and Sabatini, D.M. (2010). mTORC1 controls fasting-induced ketogenesis and its modulation by ageing. Nature *468*, 1100–1104.

19. Finck, B.N., Lehman, J.J., Leone, T.C., Welch, M.J., Bennett, M.J., Kovacs, A., Han, X., Gross, R.W., Kozak, R., Lopaschuk, G.D., and Kelly, D.P. (2002). The cardiac phenotype induced by PPARalpha overexpression mimics that caused by diabetes mellitus. J. Clin. Invest. *109*, 121–130.

20. Zhao, Y., and Srivastava, D. (2007). A developmental view of microRNA function. Trends Biochem. Sci. *32*, 189–197.

21. Chandradoss, S.D., Schirle, N.T., Szczepaniak, M., MacRae, I.J., and Joo, C. (2015). A dynamic search process underlies microRNA targeting. Cell *162*, 96–107.

22. He, Q.-Q., Xiong, L.-L., Liu, F., He, X., Feng, G.-Y., Shang, F.-F., Xia, Q.J., Wang, Y.C., Qiu, D.L., Luo, C.Z., et al. (2016). MicroRNA-127 targeting of mitoNEET inhibits neurite outgrowth, induces cell apoptosis and contributes to physiological dysfunction after spinal cord transection. Sci. Rep. *6*, 35205.

23. Chen, X., Xia, J., Xia, Z., Zhang, H., Zeng, C., Lu, C., Zhang, W., and Wang, W. (2015). Potential functions of microRNAs in starch metabolism and development revealed by miRNA transcriptome profiling of cassava cultivars and their wild progenitor. BMC Plant Biol. *15*, 33.

24. Sun, X., Sit, A., and Feinberg, M.W. (2014). Role of miR-181 family in regulating vascular inflammation and immunity. Trends Cardiovasc. Med. *24*, 105–112.

25. Niu, J., Xue, A., Chi, Y., Xue, J., Wang, W., Zhao, Z., Fan, M., Yang, C.H., Shao, Z.M., Pfeffer, L.M., et al. (2016). Induction of miRNA-181a by genotoxic treatments promotes chemotherapeutic resistance and metastasis in breast cancer. Oncogene *35*, 1302–1313.

26. Galluzzi, L., Morselli, E., Vitale, I., Kepp, O., Senovilla, L., Criollo, A., Servant, N., Paccard, C., Hupé, P., Robert, T., et al. (2010). miR-181a and miR-630 regulate cisplatin-induced cancer cell death. Cancer Res. *70*, 1793–1803.

27. Chakravarthy, M.V., Lodhi, I.J., Yin, L., Malapaka, R.R.V., Xu, H.E., Turk, J., and Semenkovich, C.F. (2009). Identification of a physiologically relevant endogenous ligand for PPARalpha in liver. Cell *138*, 476–488.

28. Zeibig, J., Karlic, H., Lohninger, A., Damsgaard, R., and Smekal, G. (2005). Do blood cells mimic gene expression profile alterations known to occur in muscular adaptation to endurance training? Eur. J. Appl. Physiol. *95*, 96–104.

29. Kar, R., Singha, P.K., Venkatachalam, M.A., and Saikumar, P. (2009). A novel role for MAP1 LC3 in nonautophagic cytoplasmic vacuolation death of cancer cells. Oncogene *28*, 2556–2568.

30. Jiao, M., Ren, F., Zhou, L., Zhang, X., Zhang, L., Wen, T., Wei, L., Wang, X., Shi, H., Bai, L., et al. (2014). Peroxisome proliferator-activated receptor α activation attenuates the inflammatory response to protect the liver from acute failure by promoting the autophagy pathway. Cell Death Dis. *5*, e1397.

31. Rieswijk, L., Brauers, K.J.J., Coonen, M.L.J., van Breda, S.G.J., Jennen, D.G.J., and Kleinjans, J.C.S. (2015). Evaluating microRNA profiles reveals discriminative responses following genotoxic or non-genotoxic carcinogen exposure in primary mouse hepatocytes. Mutagenesis *30*, 771–784.

32. Rieswijk, L., Brauers, K.J.J., Coonen, M.L.J., Jennen, D.G.J., van Breda, S.G.J., and Kleinjans, J.C.S. (2016). Exploiting microRNA and mRNA profiles generated in vitro from carcinogen-exposed primary mouse hepatocytes for predicting in vivo genotoxicity and carcinogenicity. Mutagenesis *31*, 603–615.

33. Warden, A., Truitt, J., Merriman, M., Ponomareva, O., Jameson, K., Ferguson, L.B., Mayfield, R.D., and Harris, R.A. (2016). Localization of PPAR isotypes in the adult mouse and human brain. Sci. Rep. *6*, 27618.

34. Chinetti, G., Lestavel, S., Bocher, V., Remaley, A.T., Neve, B., Torra, I.P., Teissier, E., Minnich, A., Jaye, M., Duverger, N., et al. (2001). PPAR-alpha and PPAR-gamma activators induce cholesterol removal from human macrophage foam cells through stimulation of the ABCA1 pathway. Nat. Med. *7*, 53–58.

35. Cuzzocrea, S., Di Paola, R., Mazzon, E., Genovese, T., Muià, C., Centorrino, T., and Caputi, A.P. (2004). Role of endogenous and exogenous ligands for the peroxisome proliferators activated receptors alpha (PPAR-alpha) in the development of inflammatory bowel disease in mice. Lab. Invest. *84*, 1643–1654.

36. Keller, H., Dreyer, C., Medin, J., Mahfoudi, A., Ozato, K., and Wahli, W. (1993). Fatty acids and retinoids control lipid metabolism through activation of peroxisome proliferator-activated receptor-retinoid X receptor heterodimers. Proc. Natl. Acad. Sci. USA *90*, 2160–2164.

37. Lehmann, J.M., Lenhard, J.M., Oliver, B.B., Ringold, G.M., and Kliewer, S.A. (1997). Peroxisome proliferator-activated receptors α and γ are activated by indomethacin and other non-steroidal anti-inflammatory drugs. J. Biol. Chem. *272*, 3406–3410.

38. Gocke, A.R., Hussain, R.Z., Yang, Y., Peng, H., Weiner, J., Ben, L.H., Drew, P.D., Stuve, O., Lovett-Racke, A.E., and Racke, M.K. (2009). Transcriptional modulation of the immune response by peroxisome proliferator-activated receptor-α agonists in autoimmune disease. J. Immunol. *182*, 4479–4487.

39. Peters, J.M., Shah, Y.M., and Gonzalez, F.J. (2012). The role of peroxisome proliferator-activated receptors in carcinogenesis and chemoprevention. Nat. Rev. Cancer *12*, 181–195.

40. Peters, J.M., Morales, J.L., and Gonzalez, F.J. (2011). Modulation of gastrointestinal inflammation and colorectal tumorigenesis by peroxisome proliferator-activated receptor-β/δ (PPARβ/δ). Drug Discov. Today Dis. Mech. *8*, e85–e93.

41. Pelicano, H., Carney, D., and Huang, P. (2004). ROS stress in cancer cells and therapeutic implications. Drug Resist. Updat. *7*, 97–110.

42. Lodder, J., Denaës, T., Chobert, M.-N., Wan, J., El-Benna, J., Pawlotsky, J.-M., Lotersztajn, S., and Teixeira-Clerc, F. (2015). Macrophage autophagy protects against liver fibrosis in mice. Autophagy *11*, 1280–1292.

43. Mitsopoulos, P., and Suntres, Z.E. (2010). Cytotoxicity and gene array analysis of alveolar epithelial A549 cells exposed to paraquat. Chem. Biol. Interact. *188*, 427–436.

44. Messmer, D., Lorrain, K., Stebbins, K., Bravo, Y., Stock, N., Cabrera, G., Correa, L., Chen, A., Jacintho, J., Chiorazzi, N., et al. (2015). A selective novel peroxisome proliferator–activated receptor (PPAR)-α antagonist induces apoptosis and inhibits proliferation of CLL cells in vitro and in vivo. Mol. Med. *21*, 410–419.

45. De Silva, D.S., Wilson, R.M., Hutchinson, C., Ip, P.C., Garcia, A.G., Lancel, S., Ito, M., Pimentel, D.R., and Sam, F. (2009). Fenofibrate inhibits aldosterone-induced apoptosis in adult rat ventricular myocytes via stress-activated kinase-dependent mechanisms. Am. J. Physiol. Heart Circ. Physiol. *296*, H1983–H1993.

46. Gao, J., Liu, Q., Xu, Y., Gong, X., Zhang, R., Zhou, C., Su, Z., Jin, J., Shi, H., Shi, J., and Hou, Y. (2015). PPARα induces cell apoptosis by destructing Bcl2. Oncotarget *6*, 44635–44642.

47. Zak, Z., Gelebart, P., and Lai, R. (2010). Fenofibrate induces effective apoptosis in mantle cell lymphoma by inhibiting the TNFalpha/NF-kappaB signaling axis. Leukemia *24*, 1476–1486.

48. Ouyang, M., Li, Y., Ye, S., Ma, J., Lu, L., Lv, W., Chang, G., Li, X., Li, Q., Wang, S., and Wang, W. (2014). MicroRNA profiling implies new markers of chemoresistance of triple-negative breast cancer. PLoS ONE *9*, e96228.

49. Monteys, A.M., Spengler, R.M., Wan, J., Tecedor, L., Lennox, K.A., Xing, Y., and Davidson, B.L. (2010). Structure and activity of putative intronic miRNA promoters. RNA *16*, 495–505.

50. Huang, Y., Kesselman, D., Kizub, D., Guerrero-Preston, R., and Ratovitski, E.A. (2013). Phospho-ΔNp63α/microRNA feedback regulation in squamous carcinoma cells upon cisplatin exposure. Cell Cycle *12*, 684–697.

51. Saini, H.K., Griffiths-Jones, S., and Enright, A.J. (2007). Genomic analysis of human microRNA transcripts. Proc. Natl. Acad. Sci. USA *104*, 17719–17724.

52. Ke, G., Liang, L., Yang, J.M., Huang, X., Han, D., Huang, S., Zhao, Y., Zha, R., He, X., and Wu, X. (2013). MiR-181a confers resistance of cervical cancer to radiation therapy through targeting the pro-apoptotic PRKCD gene. Oncogene *32*, 3019–3027.

53. Debernardi, S., Skoulakis, S., Molloy, G., Chaplin, T., Dixon-McIver, A., and Young, B.D. (2007). MicroRNA miR-181a correlates with morphological sub-class of acute myeloid leukaemia and the expression of its target genes in global genome-wide analysis. Leukemia *21*, 912–916.

54. Presnell, S.R., Al-Attar, A., Cichocki, F., Miller, J.S., and Lutz, C.T. (2015). Human natural killer cell microRNA: differential expression of MIR181A1B1 and MIR181A2B2 genes encoding identical mature microRNAs. Genes Immun. *16*, 89–98.

55. Wang, Y., Yu, Y., Tsuyada, A., Ren, X., Wu, X., Stubblefield, K., Rankin-Gee, E.K., and Wang, S.E. (2011). Transforming growth factor-β regulates the sphere-initiating stem cell-like feature in breast cancer through miRNA-181 and ATM. Oncogene *30*, 1470–1480.

56. Tekirdag, K.A., Korkmaz, G., Ozturk, D.G., Agami, R., and Gozuacik, D. (2013). MIR181A regulates starvation- and rapamycin-induced autophagy through targeting of ATG5. Autophagy *9*, 374–385.